A Multi-Wavelength Census of Star Formation at Redshift z~2

by

Naveen A. Reddy

ISBN: 1-58112- 331-0

DISSERTATION.COM

Boca Raton, Florida
USA • 2006

A Multi-Wavelength Census of Star Formation at Redshift z~2

Dissertation.com
Boca Raton, Florida
USA • 2006

ISBN: 1-58112- 331-0

A Multi-Wavelength Census of Star Formation at Redshift $z \sim 2$

Thesis by
Naveen A. Reddy

In Partial Fulfillment of the Requirements
for the Degree of
Doctor of Philosophy

California Institute of Technology
Pasadena, California

2006

(Defended May 15, 2006)

Abstract

We examine the census of star-forming galaxies and their extinction properties at redshift $z \sim 2$, when a large fraction of the stellar mass in the universe formed. We find a good agreement between the X-ray, radio, and de-reddened UV estimates of the average star formation rate (SFR) for our sample of $z \sim 2$ galaxies of $\sim 50\ M_{\odot}\ \mathrm{yr}^{-1}$, indicating that the locally calibrated SFR relations appear to be statistically valid from redshifts $1.5 \lesssim z \lesssim 3.0$. *Spitzer* MIPS data are used to assess the extinction properties of individual star-forming galaxies, and we find that the rest-frame UV slope of most galaxies at $z \sim 2$ can be used to infer their attenuation factors, $L_{\mathrm{bol}}/L_{\mathrm{UV}}$. As in the local universe, the obscuration, $L_{\mathrm{FIR}}/L_{\mathrm{UV}}$, is strongly dependent on bolometric luminosity, and ranges in value from < 1 to ~ 1000 within the sample considered. However, the obscuration is ~ 10 times smaller at a given L_{bol} (or, equivalently, a similar level of obscuration occurs at luminosities ~ 10 times larger) at $z \sim 2$ than at $z \sim 0$. This trend is expected as galaxies age and their gas becomes more dust-enriched. Specific SFRs indicate wide range in the evolutionary state of galaxies at $z \sim 2$, from galaxies that have just begun to form stars to those that have already accumulated most of their stellar mass and are about to become, or already are, passively evolving. Finally, we examine two techniques for assessing the census of galaxies at $z \sim 2$. In the first, we select galaxies using optical, near-IR, and sub-mm criteria, and find a large overlap between optical and near-IR selected samples of galaxies at $z \sim 2$. The second technique involves reconstructing the luminosity function of $z \sim 2$ galaxies as determined from Monte Carlo simulations. We find that the SFR density increases between $z = 4$ to 2 by a factor of ~ 1.2. However, this increase is mild compared to the much steeper increase from $z \sim 6$ to $z \sim 4$, suggesting that the processes responsible for the increase in SFR density at early epochs saturate around $z \sim 2$.

Contents

x

List of Figures

List of Tables

Chapter 1

Introduction

Understanding the star formation history and stellar mass evolution of galaxies is perhaps one of the most fundamental issues in cosmology. Observations of the stellar mass and star formation rate density, the number density of QSOs, and galaxy morphology at both low ($z \lesssim 1$) and high ($z \gtrsim 3$) redshifts indicate that most of the activity responsible for shaping the bulk properties of galaxies to their present form occured in the epochs between $1 \lesssim z \lesssim 3$ (e.g., Dickinson et al. 2003b; Rudnick et al. 2003; Chapman et al. 2005; Madau et al. 1996; Lilly et al. 1996, 1995; Steidel et al. 1999; Shaver et al. 1996; Fan et al. 2001; Di Matteo et al. 2003; Conselice et al. 2004; Papovich et al. 2003; Shapley et al. 2001; Giavalisco et al. 1996). Galaxy studies during this intermediate redshift range have suffered, however, because of our inability to identify large samples of galaxies during this critical epoch. The primary difficulty at these redshifts was due to the fact that the lines used for redshift identification are shifted into the near-UV where detector sensitivity has lagged, or to the near-IR where spectroscopy is more difficult due to higher backgrounds.

However, the advent of $8-10$ m class telescopes and improvements in detector technology have allowed us to make significant progress by making it possible to select large samples of galaxies during the critical epochs corresponding to redshifts $1.4 \lesssim z \lesssim 3.0$. There are essentially two ways in which to proceed in order to assess the census of galaxies at high redshift. The first is to observe galaxies over as wide a range in wavelengths as possible in order to select those that comprise the bulk of the total star formation rate density (SFRD). Along this line, several color criteria have been developed to target galaxies over the redshift range $1.4 \lesssim z \lesssim 3.0$. The first method, and the one upon which most of this thesis is based, is optical selection of galaxies through the $U_n G\mathcal{R}$ bands (Adelberger et al. 2004; Steidel et al. 2004). The second method is to select galaxies by their near-IR $z-K$ color, taking advantage of the fact that for redshifts $z \gtrsim 1.4$, the $z-$ and K-bands bracket the age-sensitive Balmer and 4000 Å break features in the spectra of most star-forming and "passively evolving" (or quiescent) galaxies (Daddi et al. 2004b). The third method selects either passively evolving or star-forming galaxies at redshifts $z \gtrsim 2$ based on the single color criteria $J-K_{\rm s} > 2.3$ (in Vega magnitudes), again taking advantage of the Balmer and 4000 Å breaks (Franx et al. 2003). The fourth method relies on the monochromatic flux at 850 μm to select dusty, high redshift galaxies (Blain et al. 1999). Each selection method presents its own advantages and disadvantages, but one critical issue that has previously been neglected is that one must take into account the substantial overlap between these samples when estimating the total SFRD (Reddy et al. 2005). Each of the selection criteria and their respective overlap and contributions to the SFRD are discussed in Chapter 3.

The second approach to assessing the total star formation rate density is to simulate many realizations of the intrinsic distribution of galaxy properties at high redshift, subject these realizations to the same photometric methods and selection criteria as applied to real data, and then adjust the simulated realizations until convergence is reached between the expected and observed distribution of galaxy properties. This Monte Carlo approach has the advantage, unlike the first method, of not requiring the observational effort necessary to conduct a panchromatic assessment of the total SFRD. The method works especially

well when applied to joint spectroscopic and photometric samples of galaxies and therefore works best for optically-selected samples where spectroscopy is much more feasible than for near-IR selected samples. Perhaps the main disadvantage of this method is the inability to correct sample completeness for galaxies that are completely missed (i.e., not scattered into the color selection windows). Nevertheless, applying this method to spectroscopically confirmed samples of high redshift galaxies allows one to evaluate the systematic effects of photometric scatter and the intrinsic variation in colors due to line emission and absorption with great accuracy. We can further evaluate the signficance and magnitude of the dust extinction corrections necessary to translate UV luminosities to total bolometric luminosities (see below and Chapters 2, 3, 4, and 6). Our Monte Carlo approach to computing sample incompleteness can then be used to reconstruct the total SFRD. This method is discussed in detail in Chapter 6.

1.1 The Optical Selection of High Redshift Galaxies

1.1.1 Photometric Selection

Constructing a practical set of selection criteria to select all galaxies in any desired redshift range and reject all others is an intractable problem. One extreme is to select all objects down to a given magnitude limit, such as in flux-limited surveys of high redshift galaxies, but unfortunately such studies suffer from significant amounts of foreground contamination. Without additional color criteria, one may spend 99% of the time spectroscopically confirming low redshift contaminants before assembling a significant sample of galaxies at the desired redshift range. Color-selected samples have the distinct advantage of allowing one to specifically target a desired redshift range while minimizing the number of interlopers. Perhaps the most successful of the various color criteria that have been designed to select galaxies at different epochs is rest-frame UV color selection, pioneered by Steidel et al. (1995) to select galaxies at $z \sim 3$, and extended to higher redshifts (e.g., Bouwens et al. 2005, 2004; Bunker et al. 2004; Dickinson et al. 2004; Yan et al. 2003). The success of this technique is partly due to its simplicity in that only a few broadband filters are required to assemble such samples and, at lower redshifts ($1.4 \lesssim z \lesssim 3.5$), where the galaxies can be spectroscopically observed and precise redshifts can be obtained in a short amount of observing time. Combined, these surveys have given us an unprecedented view of galaxy evolution over almost the entire age of the universe.

For the past several years, the main focus of our group has been to assemble a large sample of galaxies at the peak epoch of galaxy formation and black hole growth, corresponding to redshifts $1.5 \lesssim z \lesssim 2.6$. The selection criteria aim to select actively star-forming galaxies at $z \sim 2$ with the same range in intrinsic UV color and extinction as Lyman break galaxies (LBGs) at $z \sim 3$ (Steidel et al. 2003). While galaxies at $z \sim 2$ do not have any of the strong spectral breaks across the $U_nG\mathcal{R}$ bands used to select higher redshift galaxies (Figure 1.1), they do occupy a particular area of $U_nG\mathcal{R}$ color space that can be singled out (Figure 1.2).

We have used the "BX" criteria of Adelberger et al. (2004) and Steidel et al. (2004) to select galaxies at redshifts $2.0 \lesssim z \lesssim 2.6$, placing the following requirements on the observed colors:

$$\begin{aligned} G-\mathcal{R} &\geq -0.2 \\ U_n-G &\geq G-\mathcal{R}+0.2 \\ G-\mathcal{R} &\leq 0.2(U_n-G)+0.4 \\ U_n-G &\leq G-\mathcal{R}+1.0. \end{aligned} \tag{1.1}$$

Similarly we have selected "BM" galaxies at redshifts $1.5 \lesssim z \lesssim 2.0$ using the following criteria:

$$G-\mathcal{R} \geq -0.2$$

$$\begin{aligned} U_n - G &\geq G - \mathcal{R} - 0.1 \\ G - \mathcal{R} &\geq 0.2(U_n - G) + 0.4 \\ U_n - G &\leq G - \mathcal{R} + 0.2. \end{aligned} \tag{1.2}$$

To ensure a sample of galaxies amenable to spectroscopic followup, we imposed a magnitude limit of $\mathcal{R} = 25.5$. This limit corresponds to an absolute magnitude 0.6 mag fainter at $z = 2.2 \pm 0.4$ (the mean and dispersion of the measured redshift distribution for BX candidates with $z > 1$) than at $z \sim 3$. We also excluded candidates with $\mathcal{R} < 19$ since almost all of these objects are stars. Given the constraints of the color criteria and the self-imposed magnitude limits, the combined BM, BX, and LBG samples constitute 25 to 30% of the total $\mathcal{R}$ and K_s band counts to $\mathcal{R} = 25.5$ and $K_s(AB) = 24.4$, respectively.

1.1.2 Spectroscopic Followup

The spectroscopic followup to the optically selected sample is discussed in detail in the following chapters. Briefly, we took advantage of the multi-object capabilities of the Keck LRIS (Low Resolution Imaging Spectrograph; Oke et al. 1995) instrument to obtain spectroscopy. The unrivaled near-UV sensitivity of the blue arm of LRIS (LRIS-B; Steidel et al. 2004) is necessary for spectroscopically identifying galaxies in the so-called spectroscopic desert where BX and BM selected galaxies are expected to lie and where the stellar and interstellar absorption lines typically used for redshift identification are shifted into the near-UV. The spectroscopic sample presently consists of 104 BM, 1125 BX, and 1444 LBG galaxies (spread throughout multiple uncorrelated fields), with mean spectroscopic redshifts of $\langle z \rangle = 1.72 \pm 0.34$, $\langle z \rangle = 2.20 \pm 0.32$, and $\langle z \rangle = 2.96 \pm 0.26$, for the BM, BX, and LBG samples, respectively (Figure 1.3). It is the spectroscopic samples at $z \sim 2$ (BM and BX) that form the basis of the work presented in Chapters 2, 3, 4, and 5. In Chapter 6, we consider the joint photometric and spectroscopic samples to compute the luminosity function and the contribution of optically-selected galaxies to the total star formation rate density at $z \sim 2$.

1.2 Bolometric Measures of Star Formation Rates

Estimating the star formation rates of galaxies based on a single monochromatic flux (or even broadband SEDs) entails many assumptions, some of which have been tested and others which have not. For example, one must assume a particular form of the initial mass function (IMF) of stars in order to estimate a star formation rate, but directly measuring the IMF is very difficult for everything except local global clusters where stars can be individually resolved. Another assumption that was previously untested at high redshift is the relationship between the observed UV luminosities of star forming galaxies and their total bolometric luminosities. Prior to the advent of large-scale multi-wavelength surveys, it was common to make untested extinction corrections to galaxies in UV surveys based on relationships established locally. The situation has changed significantly with panchromatic surveys which have allowed us to examine the extinction free measures of star formation rates in high redshift galaxies and compare these estimates with the observed UV emission, as discussed in Chapters 2 and 4. Combining our census of the star-forming galaxy population at high redshift and our intimate knowledge of the extinction corrections required to estimate bolometric SFRs, we can now make assertions regarding the star formation history and buildup of stellar mass in the Universe with much more confidence than previously possible.

1.3 Outline of the Thesis

The outline of this thesis is as follows. In the next chapter, we use deep X-ray and radio emission as independent probes of the star formation rates and bolometric activity in galaxies at $z \sim 2$. While the X-

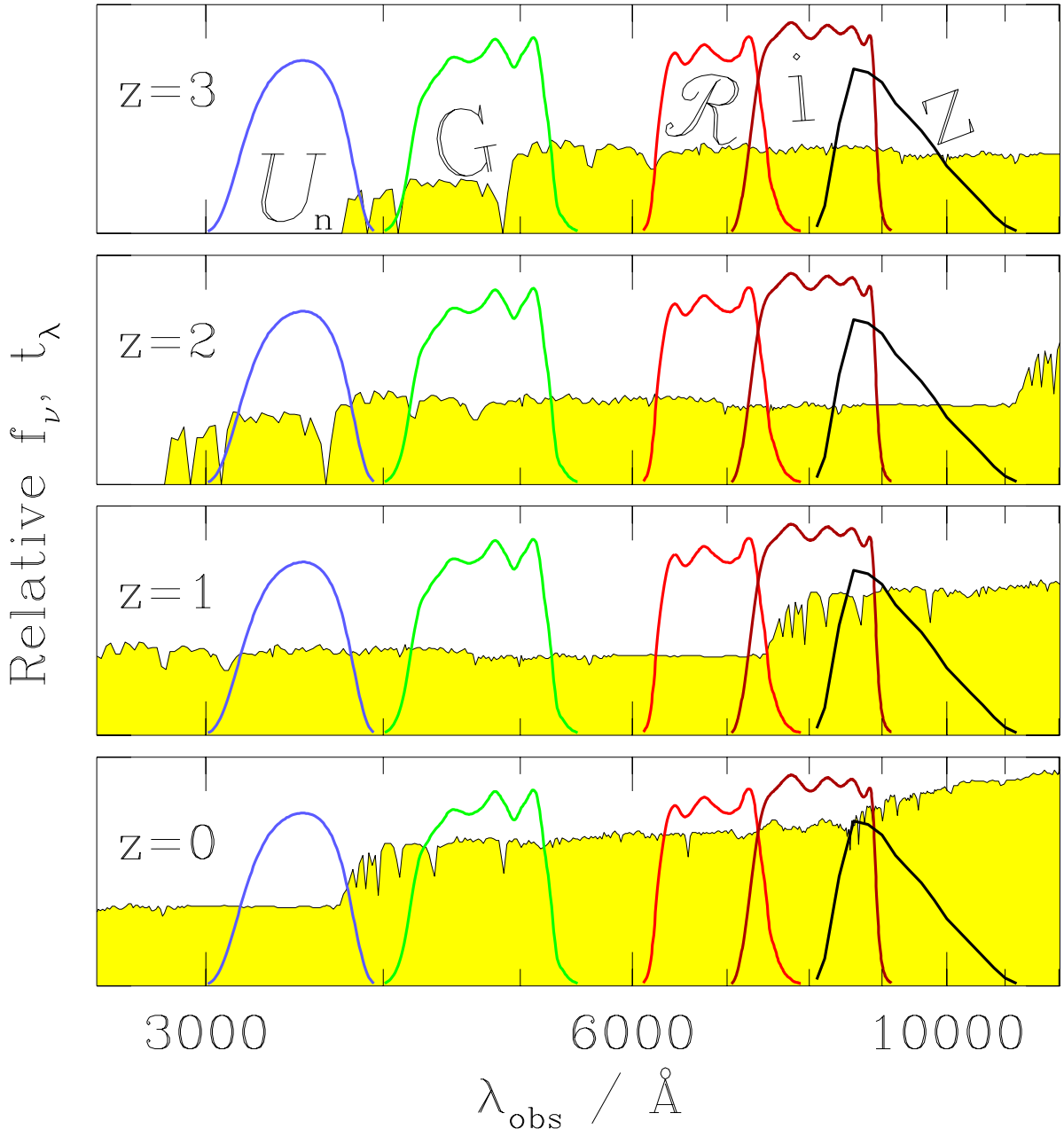

Figure 1.1 Relative placement of the $U_nG\mathcal{R}Iz$ bands with respect to a constant star forming galaxy at redshifts $z = 0 - 4$ (figure from Adelberger et al. 2004).

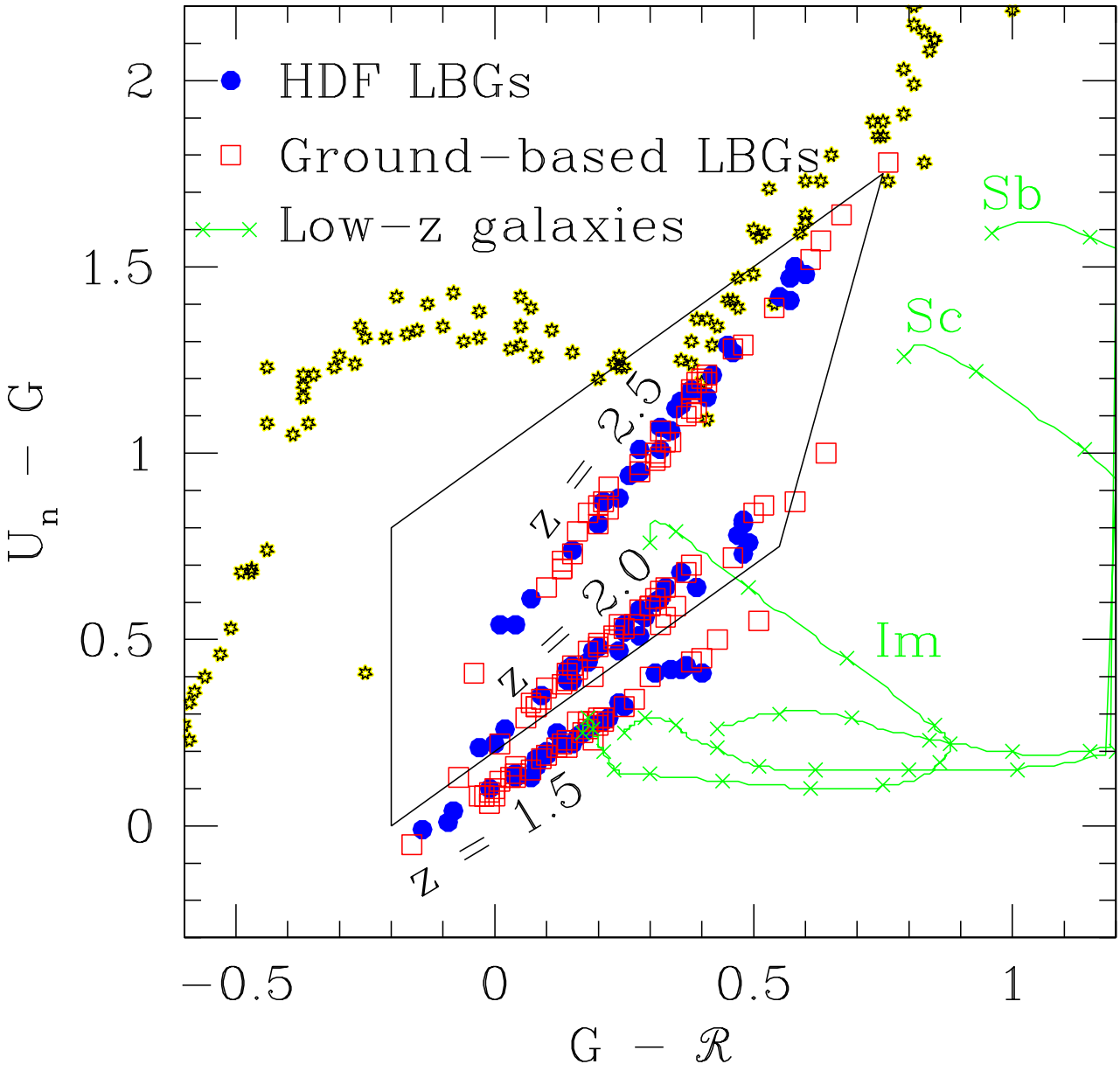

Figure 1.2 Expected $U_nG\mathcal{R}$ colors of stars (stars; from Gunn & Stryker 1983) and star-forming galaxies at redshifts $z = 1.5$, 2.0, and 2.5 (blue circles and red squares; data from Papovich et al. 2001 and Shapley et al. 2001). Green tracks indicate the colors of galaxies of different spectral types (Im, Sb, Sc), proceeding from $z = 0$ to $z = 1.5$, in intervals of $\delta z = 0.1$ as denoted by the crosses. The trapezoid denotes the BX selection window, as defined by Equation 1.1, which is designed to include as many galaxies at redshifts $2.0 \lesssim z \lesssim 2.6$ while excluding stars and low redshift $z < 1.5$ galaxies (figure from Adelberger et al. 2004).

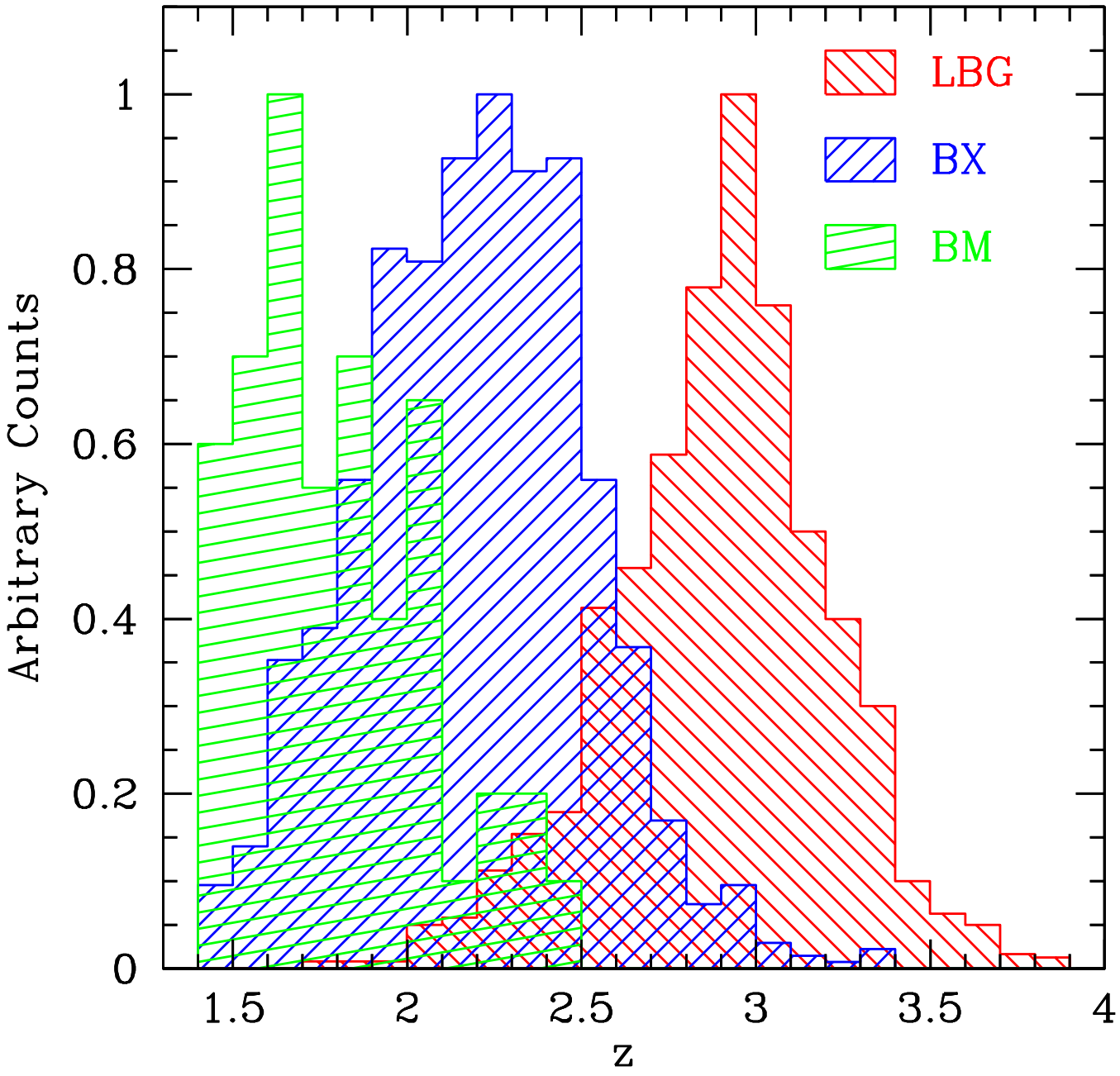

Figure 1.3 Arbitrarily normalized spectroscopic redshift distributions of galaxies with $z > 1.4$ in the BM, BX, and LBG samples. The total number of galaxies represented here is 2673.

ray and radio data are not sufficiently sensitive to detect most optically-selected galaxies at these redshifts, we can use stacking analyses to infer important information regarding the average star formation rates of well-selected subsamples of galaxies. In Chapter 3, we perform a detailed comparison of galaxies selecting using optical, near-IR, and sub-mm criteria. We quantify the overlap between these samples and, using stacked X-ray emission, demonstrate that this sample overlap must be taken into account when estimating the total star formation rate density. We extend the results of the census of star-forming galaxies presented in Chapter 3 by examining the rest-frame infrared emission from $z \sim 2$ galaxies selected in various ways. We also discuss how the average extinction factors for galaxies of a given luminosity change as a function of redshift, from $z \sim 2$ to $z = 0$. We go on to show how bolometric measures of the star formation rates of galaxies, combined with stellar mass estimates from population synthesis modelling, can be used to deduce the evolutionary state of galaxies in terms of their propensity for future star formation. In Chapter 5 we discuss in detail the spectroscopic sample of optically-selected galaxies in the GOODS-North field (Giavalisco et al. 2004b; Dickinson et al. 2003a), which is the basis for the work presented in Chapters 2, 3, and 4. Using multi-wavelength data in this field, we examine the properties of obscured AGN in optically-selected host galaxies. Finally, in Chapter 6, we use sophisticated Monte Carlo analysis of our joint photometric and spectroscopic samples of galaxies in the $z \sim 2$ survey (e.g., Adelberger et al. 2004; Steidel et al. 2004) to estimate the effects of photometric scattering, Lyman-alpha line perturbations, and other systematic effects introduced by the optical selection of star-forming galaxies at redshift $z \sim 2$. We use these results to construct the luminosity function at $z \sim 2$, and incorporating our knowledge of extinction, to estimate the total star formation rate density and the implications for the star formation history and buildup of stellar mass in the Universe. Finally, in the epilogue, we discuss several unresolved but important issues to consider for obtaining even more stringent constraints on the cosmic star formation history, as well as determining the evolutionary paths of individual galaxies.

Chapter 2

X-Ray and Radio Emission from UV-Selected Star Forming Galaxies at Redshifts $1.5 \lesssim Z \lesssim 3.0$ in the GOODS-North Field*†

Naveen A. Reddy & Charles C. Steidel

California Institute of Technology, MS 105–24, Pasadena, CA 91125; nar@astro.caltech.edu, ccs@astro.caltech.edu

Abstract

We have examined the stacked radio and X-ray emission from UV-selected galaxies spectroscopically confirmed to lie between redshifts $1.5 \lesssim z \lesssim 3.0$ in the GOODS-North field to determine their average extinction and star formation rates (SFRs). The X-ray and radio data are obtained from the Chandra 2 Msec survey and the Very Large Array, respectively. There is a good agreement between the X-ray, radio, and de-reddened UV estimates of the average SFR for our sample of $z \sim 2$ galaxies of ~ 50 $M_\odot$ yr^{-1}, indicating that the locally calibrated SFR relations appear to be statistically valid from redshifts $1.5 \lesssim z \lesssim 3.0$. We find that UV-estimated SFRs (uncorrected for extinction) underestimate the bolometric SFRs as determined from the 2 to 10 keV X-ray luminosity by a factor of ~ 4.5 to 5.0 for galaxies over a large range in redshift from $1.0 \lesssim z \lesssim 3.5$.

2.1 Introduction

Estimating global star formation rates (SFRs) of galaxies typically requires using relations that can be quite uncertain as they incorporate a large number of assumptions in converting between specific and bolometric luminosities (e.g., assumed IMF, extinction, etc.; e.g., Adelberger & Steidel 2000). The varied efforts in the Great Observatories Origins Deep Survey (GOODS; Giavalisco et al. 2004b) allow us to examine the same galaxies over a broad range of wavelengths to mitigate some of these uncertainties. X-ray, radio, and UV emission are all thought to result directly from massive stars and are consequently used as tracers of current star formation (e.g., Ranalli et al. 2003; Condon 1992; Gallego et al. 1995). Here we use the X-ray, radio, and UV emission, each differently affected by extinction (or not at all), to determine SFRs of galaxies at $z \sim 2$.

*Based on data obtained at the W. M. Keck Observatory, which is operated as a scientific partnership among the California Institute of Technology, the University of California, and NASA, and was made possible by the generous financial support of the W. M. Keck Foundation.

†A version of this chapter was published in *The Astrophysical Journal*, vol. 603, 13–16.

Observations of the QSO and stellar mass density, and morphological diversification all point to the epoch around $z \sim 2$ as an important period in cosmic history (e.g., Di Matteo et al. 2003; Chapman et al. 2003). Until recently, this epoch has been largely unexplored as lines used for redshift identification are shifted to the near-UV, where detector sensitivity has been poor or to the near-IR, where spectroscopy is more difficult due to higher backgrounds. With the recent commissioning of the blue side of the Low Resolution Imaging Spectrograph (LRIS; Oke et al. 1995) on the Keck I telescope, we have for the first time been able to obtain spectra for large numbers of galaxies at these redshifts. Adding to the multi-wavelength efforts in the GOODS-North field, we have undertaken a program to identify photometric candidates in this field between $1.5 \lesssim z \lesssim 3.0$ and perform followup spectroscopy with LRIS-B (Steidel et al. 2004). This UV-selected sample of galaxies forms the basis for our subsequent multi-wavelength analysis.

Current sensitivity limits at X-ray and radio wavelengths preclude the direct detection of normal star forming galaxies at $z \gtrsim 1.5$. Nonetheless, we can use a "stacking" procedure to add the emission from a class of objects in order to determine their average emission properties (e.g., Nandra et al. 2002; Brandt et al. 2001; Seibert et al. 2002). In this paper, we present a stacking analysis of the radio and X-ray emission from UV-selected star forming galaxies at redshifts $1.5 \lesssim z \lesssim 3.0$ to cross-check three different techniques of estimating SFRs at high redshifts. $H_o = 70$ km s^{-1} Mpc^{-1}, $\Omega_{\rm M} = 0.3$, and $\Omega_\Lambda = 0.7$ are assumed throughout.

2.2 Data

The techniques for selecting galaxies at $z \sim 2$ are designed to cover the same range of UV properties and extinction to those used to select Lyman-break galaxies (LBGs) at higher redshifts ($z \gtrsim 3.0$; Adelberger et al. 2004). Here, we simply mention that we have two spectroscopic samples at $1.5 \lesssim z \lesssim 2.5$: a "BX" sample of galaxies selected on the expected $U_{\rm n}G\mathcal{R}$ colors of LBGs de-redshifted to $2.0 \lesssim z \lesssim 2.5$; and a "BM" sample targeting $z \sim 1.5 - 2.0$. (see Adelberger et al. 2004; Steidel et al. 2004 for a complete description). We presently have 138 redshifts ($\langle z \rangle \sim 2.2 \pm 0.3$) and 48 redshifts ($\langle z \rangle \sim 1.7 \pm 0.3$) in the GOODS-North BX and BM samples, respectively.

The X-ray data are from the Chandra 2 Msec survey of the GOODS-North region (Alexander et al. 2003). We made use of their raw images and exposure maps in the Chandra soft X-ray band ($0.5-2.0$ keV). Dividing the raw image by the appropriate exposure map yields an image with the count rates corrected for vignetting, exposure time, and variations in instrumental sensitivity. The on-axis soft band sensitivity is $\sim 2.5 \times 10^{-17}$ ergs cm^{-2} s^{-1} ($3\,\sigma$).

The radio data are from the Richards (2000) Very Large Array (VLA) survey of the Hubble Deep Field North (HDF-N), reaching a $3\,\sigma$ sensitivity of $\sim 23\,\mu$Jy beam^{-1} at 1.4 GHz. The final naturally weighted image has a pixel size of $0\farcs4$ and resolution of $2\farcs0$, with astrometric accuracy of $< 0\farcs03$.

2.3 Stacking Procedure

We divided the spectroscopic data into subsets based on selection (BX and BM) and redshift, removed sources with matching X-ray or radio counterparts within $2\farcs5$ (or sources whose apertures are large enough to contain emission from a nearby extended X-ray or radio source), and stacked galaxies in these subsets. Four of the removed x-ray/radio sources are detected at 850 μm with the Submillimeter Common-User Bolometer Array (SCUBA).

The X-ray data were stacked using the following procedure. We added the flux within apertures randomly dithered by $0\farcs5$ at the positions of the galaxies (targets) in the X-ray images to produce a signal. Similarly sized apertures were randomly placed within $5''$ of the galaxy positions to sample the local background near each galaxy while avoiding known X-ray sources. This was repeated 1000 times to

estimate the mean signal and background. The Chandra PSF widens for large angles from the average pointing (off-axis angle), and we fixed the aperture sizes to the 50% encircled energy (EE) radii (Feigelson et al. 2002) for off-axis angles $> 6'$. Background included at large off-axis angles becomes significant due to increasing aperture size and this can degrade the total stacked signal. Consequently, we only stacked galaxies within the off-axis angle that results in the highest S/N (this varies for each subsample, from 6 to $8'$). Including all sources in the stack reduces the S/N but does not affect the absolute flux value. For sources $< 6'$ from the pointing center, the 50% EE radius falls below $2''.5$, and we adopted a fixed $2''.5$ radius aperture to avoid the possibility of placing an aperture off a target as a result of dithering or astrometric errors—which are $\sim 0''.3$—for sources very close to the average pointing. Stacking was performed on both the raw and normalized images to calculate the S/N and total count rate, respectively. Aperture corrections were applied to the raw counts and count rate. The conversion between count rate and flux was determined by averaging the count rate to flux conversions for the 74 optically bright X-ray sources in Table 7 of Alexander et al. (2003) that are assumed to have a photon index of $\Gamma = 2.0$, typical of the X-ray emission from star forming regions (e.g., Kim et al. 1992; Nandra et al. 2002), and incorporate corrections for the QE degredation of the ACIS-I chips. In converting flux to rest-frame luminosity, we assume $\Gamma = 2.0$ and a Galactic absorption column density of $N_{\rm H} = 1.6 \times 10^{20}$ cm^{-2} (Stark et al. 1992). Uncertainties in flux and luminosity are dominated by Poisson noise and not the dispersion in measured values for each stacking repetition, so we assume the former.

To stack the radio data, we extracted subimages at the locations of the targets from the mosaicked radio data of Richards (2000). These were corrected for the primary beam attenuation of the VLA with a maximum gain correction of 15%, coadded using a $1/\sigma^2$ weighted average to produce a stacked signal with maximal $S/N \sim 4.5$, and smoothed by $1''.5$. The integrated flux density, $S_{1.4\,\rm GHz}$, and error were computed from the standard AIPS[1] task JMFIT using an elliptical gaussian to model the stacked emission. We assume a synchrotron spectral index of $\gamma = -0.8$, typical of the non-thermal radio emission from star-forming galaxies (Condon 1992). Results of the X-ray and radio stacks for various subsamples are presented in Table 2.1. Four subsamples contain too few sources to yield a robust estimate of the stacked radio flux.

2.4 Results and Discussion

2.4.1 SFR Estimates

The relations established at $z = 0$ to convert luminosities to SFRs for our $z \sim 2$ sample are adopted from the following sources: Kennicutt (1998a,b) for conversion of the $1500 - 2800$ Å luminosity; Ranalli et al. (2003) for the $2 - 10$ keV luminosity; and Yun et al. (2001) for the 1.4 GHz luminosity. These relations must be used with caution when applied to individual galaxies given uncertainties in the SFR relations (e.g., burst age, IMF) as well as the factor of ~ 2 dispersion in the correlations between different specific luminosities. However, they should yield reasonable results when applied to an ensemble of galaxies, as we have done here.

Table 2.2 shows the SFR estimates based on the $2 - 10$ keV ("$\rm SFR_X$"), 1.4 GHz ("$\rm SFR_{1.4\ GHz}$"), and UV ("$\rm SFR_{UV}$") luminosities, with typical error of $\sim 20\%$. We approximate the UV luminosity by using the 1600 Å rest-frame flux for all samples except the highest redshift bin sample ($2.5 < z \lesssim 3.0$) where we use the 1800 Å rest-frame flux. UV-estimated SFRs were corrected for extinction using the observed $G - \mathcal{R}$ colors, a spectral template assuming constant star formation for $> 10^8$ yr (after which the UV colors are essentially constant), and applying the reddening law of Calzetti et al. (2000) and Meurer et al. (1999). We created four additional subsamples of galaxies according to de-reddened UV-estimated SFR,

[1]AIPS is the Astronomical Image Processing System software package written and supported by the National Radio Astronomy Observatory.

also shown in Table 2.2.

2.4.2 Stacked Galaxy Distribution and AGN

Stacking only indicates the average emission properties of galaxies, not their actual distribution, and the observed signal may result from a few luminous sources lying just below the detection threshold. To investigate this, we plot the average distribution in counts for the sample of 147 stacked spectroscopic galaxies (Figure 2.1). Much of the high-end tail of the distribution results from random positive fluctuations. Only three sources consistently had > 7 counts. Removing those objects whose apertures have > 6 counts still results in a stacked signal with $S/N \sim 2.5$ and an average loss of 21 galaxies ($\sim 14\%$ of the sample). It is therefore likely that most of the stacked galaxies contribute to the signal, particularly given their wide range in optical, and likely X-ray, properties.

Contribution of low luminosity AGNs to the stacked signal is a concern. This is a problem with most X-ray stacking analyses, but we also possess the UV spectra for our sources. There are two objects undetected in X-rays for which the UV spectra show emission lines consistent with an AGN. Our ability to identify AGNs from their UV spectra regardless of their X-ray properties, and having identified only 2 such objects out of 149, suggests that subthreshold luminous AGNs do not contribute significantly to the stacked X-ray flux. Furthermore, UV selection biases against the dustiest sources so we do not expect to find many Compton-thick AGNs in our sample.

There are also two BM galaxies coincident with known radio sources that are not detected in X-rays and are not included in the stacked samples. Removing such objects ensures excluding radio-loud AGN that might have unassuming UV and X-ray properties. For comparison, the 3 σ radio sensitivity is sufficient to detect SFR$\gtrsim 170$ $M_\odot$ yr^{-1}, a factor of 4 higher than the median SFR of our sample based on the X-ray or de-reddened UV SFR estimates. The stacked X-ray emission indicates a SFR of ~ 42 $M_\odot$ yr^{-1}. The on-axis soft-band flux limit implies a sensitivity to SFR$\gtrsim 186$ $M_\odot$ yr^{-1} at $z \sim 2$, a factor of 4.5 higher than the average SFR for spectroscopic $z \sim 2$ galaxies. Stacking the radio flux for the full spectroscopic sample indicates average SFRs from $33 - 70$ $M_\odot$ yr^{-1} depending on which estimator is used: the Bell (2003), Condon (1992), and Yun et al. (2001) calibrations give low, high, and median (~ 56 $M_\odot$ yr^{-1}) values, assuming $\gamma = -0.8$. We adopted the Yun et al. (2001) calibration as it is most relevant to the radio luminosity range considered here.

2.4.3 Bolometric Properties of $z \sim 2$ Galaxies

The UV-implied reddening indicates $A_V \sim 0.5$ mag and $N_H \sim 7.5 \times 10^{20}$ cm^{-2} assuming the Galactic calibration (Diplas & Savage 1994). For this column density, absorption in the $2-10$ keV band is negligible, and we therefore assume that SFR$_X$ is indicative of the bolometric SFR. In this case, we find a good agreement between the SFRs determined from the X-ray, radio, and de-reddened UV luminosities (L_X, $L_{1.4\ \mathrm{GHz}}$, and L_{UV}), suggesting that the locally calibrated relations between specific luminosity and SFR remain valid within the uncertainties at $z \sim 2$, under the caution that we cannot independently test for these relations as we have no direct measure of L_{bol}.

The $\langle L_X \rangle$ and $\langle L_{1.4\ \mathrm{GHz}} \rangle$ of spectroscopically identified $z \sim 2$ galaxies are comparable to those of local starbursts. The X-ray/FIR relation for local galaxies (Ranalli et al. 2003) implies $\langle L_{FIR} \rangle \sim 2.6 \times 10^{11}$ $L_\odot$. The stacked $L_{1.4\ \mathrm{GHz}}$ implies $\langle L_{FIR} \rangle = 1.1 \times 10^{11}$ $L_\odot$ (Yun et al. 2001). These estimates are similar to the FIR luminosity of luminous infrared galaxies (LIRGs), and are expected to have $S_{850\mu m} \sim 0.3$ mJy (e.g., Webb et al. 2003) and would therefore be missing in confusion-limited SCUBA surveys to 2 mJy. *Spitzer* will have the same rest-frame 7 μm sensitivity to $z \sim 2$ galaxies as ISO has at $z \sim 1$ for $L_{FIR} \gtrsim 5 \times 10^{10}$ $L_\odot$ galaxies (Weedman et al. 2004; Flores et al. 1999). Therefore, unlike the stacked averages presented here, the *Spitzer* data will be the first extinction-free tracer of the SFR distribution of the $z \sim 2$ sample as the

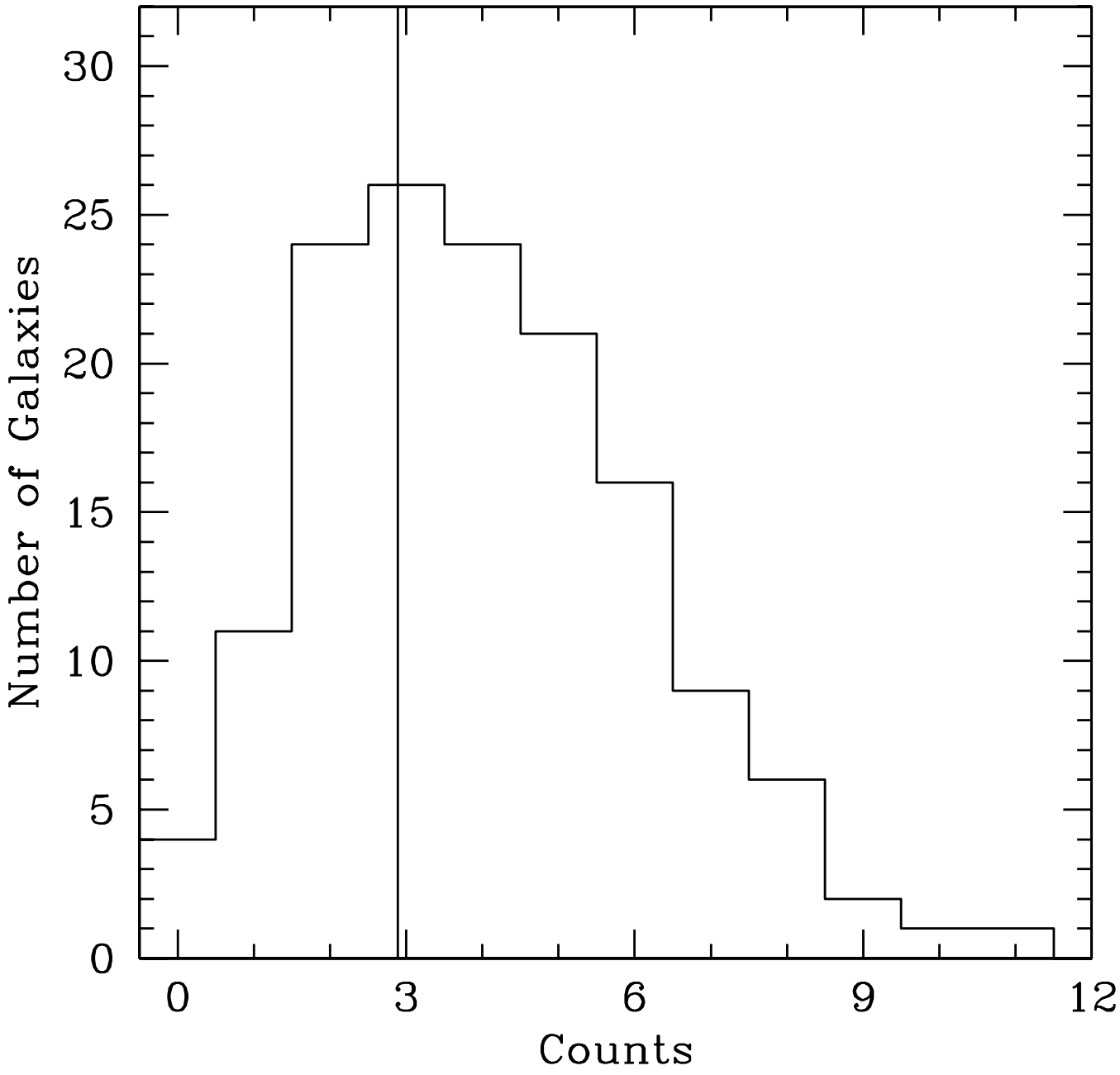

Figure 2.1 Average distribution of counts for the spectroscopic sample. The vertical line denotes the average background count per aperture. The number excess at high counts (> 7) results from random positive fluctuations.

stacked galaxies should be individually detected at 24 μm.

For a fair comparison between the three redshift bins for $1.5 < z \lesssim 3.0$, we have added back those direct X-ray detections in the stacks for the $1.5 < z \leq 2.0$ and $2.0 < z \leq 2.5$ samples that would not have been detected if they had $z > 2.5$. There were no such sources with $1.5 < z \leq 2.0$ and only one with $2.0 < z \leq 2.5$, increasing $\langle L_{2-10\ \mathrm{keV}} \rangle$ by 2% to 2.38×10^{41} ergs s^{-1}.

The distance independent ratio $\mathrm{SFR_X/SFR_{UV}^{\mathit{uncor}}}$ (Table 2.2) is similar among the selection and redshift subsamples indicating that on average *UV-estimated SFRs (uncorrected for extinction) are a factor of* ~ 4.5 *times lower than the bolometric SFRs for galaxies between redshifts* $1.5 < z \leq 3.0$. For comparison, Nandra et al. (2002) find this factor to be ~ 5 for both the $z \sim 1$ BBG and $z \sim 3$ LBG populations, and the factor is comparable to that of local starburst galaxies (Seibert et al. 2002). The attenuation computed for the BX/BM sample using the Calzetti et al. (2000) extinction law is similar to that computed from $\mathrm{SFR_X/SFR_{UV}^{\mathit{uncor}}}$. The de-reddened UV-estimated SFRs ($\mathrm{SFR_{UV}^{\mathit{cor}}}$) agree well with those predicted from the radio continuum for the two samples for which radio estimates could be obtained. Finally, we note the factor of ~ 5 UV attenuation is similar to that advocated by Steidel et al. (1999) for UV-selected samples at all redshifts.

The average attenuation factor increases as the SFR increases, as shown by the last four subsamples in Table 2.2, and is expected if galaxies with higher SFRs have greater dust content on average (Adelberger & Steidel 2000). $\mathrm{SFR_{UV}^{\mathit{cor}}}$ follows the bolometric SFR even for low luminosity systems, indicating that the observed correlations are not entirely driven by only the most luminous galaxies.

2.5 Conclusions

We have made significant progress in estimating and comparing SFRs determined from UV, X-ray, and radio emission from galaxies between redshifts $1.5 \lesssim z \lesssim 3.0$, postulated to be the most "active" epoch for galaxy evolution. The locally calibrated SFR relations, though uncertain in individual systems, appear to remain statistically valid at high redshift. Stacking the X-ray and radio emission from UV-selected galaxies at $z \sim 2$ indicates that these galaxies have an average SFR of ~ 50 M$_\odot$ yr^{-1} and an average UV attenuation factor of ~ 4.5. The prospect of increased radio sensitivity with the E-VLA, as well as X-ray campaigns in different fields to similar depth as the 2 Msec survey in the GOODS-North field, will allow for a more direct probe of the radio and X-ray flux distribution for the stacked galaxies. *Spitzer* MIPS 24 μm data for the GOODS-N field will trace the dusty star formation in $z \sim 2$ galaxies and allow for the cross-checking of the results presented here.

We thank Alice Shapley, Dawn Erb, Matt Hunt, and Kurt Adelberger for help in obtaining the data presented here. CCS has been supported by grants AST 0070773 and 0307263 from the National Science Foundation (NSF) and by the David and Lucile Packard Foundation. NAR acknowledges support from an NSF Graduate Research Fellowship.

Table 2.1. Radio and X-ray Stacking Results

Sample	N_s[a]	$\langle z \rangle$[b]	S/N[c]	$F_{0.5-2.0\,\mathrm{keV}}$[d] ($\times 10^{-18}$ ergs cm^{-2} s^{-1})	$L_{2.0-10\,\mathrm{keV}}$[e] ($\times 10^{41}$ ergs s^{-1})	$S_{1.4\,\mathrm{GHz}}$[f] (μJy)	$L_{1.4\,\mathrm{GHz}}$[g] ($\times 10^{22}$ W Hz^{-1})	νL_ν[h] ($\times 10^{10}$ L$_\odot$)
BX+BM	147	2.09	8.9	5.65 ± 0.68	2.11 ± 0.25	2.30 ± 0.65	5.90 ± 1.66	3.50
BX	109	2.22	6.8	4.83 ± 0.79	2.09 ± 0.34	2.09 ± 0.75	6.17 ± 2.21	3.86
BM	38	1.71	6.0	8.04 ± 1.34	1.84 ± 0.31	...	...	2.46
$1.5 < z \leq 2.0$	54	1.82	5.6	6.89 ± 1.27	1.84 ± 0.33	...	...	2.81
$2.0 < z \leq 2.5$	73	2.24	6.0	5.24 ± 0.96	2.33 ± 0.43	...	...	4.05
$2.5 < z \leq 3.0$	43	2.87	3.3	4.21 ± 1.46	3.40 ± 1.18	...	...	4.61

[a]Number of galaxies stacked

[b]Mean redshift

[c]Signal-to-noise calculated in a manner analogous to that in Nandra et al. 2002

[d]Average soft-band X-ray flux per object

[e]Average rest-frame X-ray luminosity per object, assuming $\Gamma = 2.0$ and $N_\mathrm{H} = 1.6 \times 10^{20}$ cm^{-2}, for our adopted cosmology

[f]Average integrated radio flux density per object

[g]Average rest-frame 1.4 GHz luminosity per object, assuming synchrotron spectral index of $\gamma = -0.8$

[h]Average UV luminosity computed from G and $\mathcal{R}$ magnitudes approximating the 1600 and 1800 Å fluxes, respectively.

Table 2.2. Star Formation Rate Estimates

Sample	SFR_X ($M_\odot$ yr^{-1})	SFR_R ($M_\odot$ yr^{-1})	SFR_{UV}^{cor} ($M_\odot$ yr^{-1})	SFR_X/SFR_{UV}^{uncor}
BX+BM	42	56	50	4.5
BX	42	58	54	4.2
BM	37	...	38	4.8
$1.5 < z \leq 2.0$	37	...	49	4.3
$2.0 < z \leq 2.5$	47	...	57	4.4
$2.5 < z \leq 3.0$	68	...	70	4.7
$SFR_{UV}^{cor} \leq 20$ $M_\odot$ yr^{-1}	14	...	11	2.3
$20 < SFR_{UV}^{cor} \leq 40$ $M_\odot$ yr^{-1}	40	...	38	4.4
$40 < SFR_{UV}^{cor} \leq 60$ $M_\odot$ yr^{-1}	44	...	48	4.7
$SFR_{UV}^{cor} > 60$ $M_\odot$ yr^{-1}	72	...	73	5.1

Chapter 3

A Census of Optical and Near-Infrared Selected Star-Forming and Passively Evolving Galaxies at Redshift $z \sim 2$*†

Naveen A. Reddy,[a] Dawn K. Erb,[b] Charles C. Steidel,[a] Alice E. Shapley,[c] Kurt L. Adelberger,[d] & Max Pettini[e]

[a]California Institute of Technology, MS 105–24, Pasadena, CA 91125

[b]Harvard-Smithsonian Center for Astrophysics, 60 Garden Street, Cambridge, MA 02138

[c]Astronomy Department, University of California, Berkeley, 601 Campbell Hall, Berkeley, CA 94720

[d]McKinsey & Company, 1420 Fifth Avenue, Suite 3100, Seattle, WA 98101

[e]Institute of Astronomy, Madingley Road, Cambridge CB3 OHA, UK

Abstract

Using the extensive multi-wavelength data in the GOODS-North field, including our ground-based rest-frame UV spectroscopy and near-IR imaging, we construct and draw comparisons between samples of optical and near-IR selected star-forming and passively evolving galaxies at redshifts $1.4 \lesssim z \lesssim 2.6$. We find overlap at the $70-80\%$ level in samples of $z \sim 2$ star-forming galaxies selected by their optical ($U_{\rm n}G\mathcal{R}$) and near-IR (BzK) colors when subjected to common K-band limits. Deep *Chandra* data indicate a $\sim 25\%$ AGN fraction among near-IR selected objects, much of which occurs among near-IR bright objects ($K_{\rm s} < 20$; Vega). Using X-rays as a proxy for bolometric star formation rate (SFR) and stacking the X-ray emission for the remaining (non-AGN) galaxies, we find the SFR distributions of $U_{\rm n}G\mathcal{R}$, BzK, and $J-K_{\rm s} > 2.3$ galaxies (i.e., Distant Red Galaxies; DRGs) are very similar as a function of $K_{\rm s}$, with $K_{\rm s} < 20$ galaxies having $\langle SFR \rangle \sim 120\ M_{\odot}\ {\rm yr}^{-1}$, a factor of 2 to 3 higher than those with $K_{\rm s} > 20.5$. The absence of X-ray emission from the reddest DRGs and BzK galaxies with $(z-K)_{\rm AB} \gtrsim 3$ indicates they must have declining star formation histories to explain their red colors and low SFRs. While the M/L ratio of passively-evolving galaxies may be larger on average, the *Spitzer*/IRAC data indicate that their inferred

*Based, in part, on data obtained at the W. M. Keck Observatory, which is operated as a scientific partnership among the California Institute of Technology, the University of California, and NASA, and was made possible by the generous financial support of the W. M. Keck Foundation.

†A version of this chapter was published in *The Astrophysical Journal*, vol. 633, 748–767.

stellar masses do not exceed the range spanned by optically selected galaxies, suggesting that the disparity in current SFR may not indicate a fundamental difference between optical and near-IR selected massive galaxies ($M^* > 10^{11}$ M$_\odot$). We consider the contribution of optical, near-IR, and submillimeter-selected galaxies to the star formation rate density (SFRD) at $z \sim 2$, taking into account sample overlap. The SFRD in the interval $1.4 \lesssim z \lesssim 2.6$ of $U_{\rm n}G\mathcal{R}$ and BzK galaxies to $K_{\rm s} = 22$, and DRGs to $K_{\rm s} = 21$ is $\sim 0.10 \pm 0.02$ $M_\odot$ yr^{-1} Mpc^{-3}. Optically-selected galaxies to $\mathcal{R} = 25.5$ and $K_{\rm s} = 22.0$ account for $\sim 70\%$ of this total. Greater than 80% of radio-selected submillimeter galaxies to $S_{850\mu{\rm m}} \sim 4$ mJy with redshifts $1.4 < z < 2.6$ satisfy either one or more of the BX/BM, BzK, and DRG criteria.

3.1 Introduction

A number of surveys have been developed to select galaxies at $z \sim 2$, determine their bolometric star formation rates (SFRs), and compare with other multi-wavelength studies to form a census of the total star formation rate density (SFRD) at $z \sim 2$ (e.g., Steidel et al. 2004; Rubin et al. 2004; Daddi et al. 2004b). A parallel line of study has been to compare optical and near-IR selected galaxies that are the plausible progenitors of the local population of passively evolving massive galaxies. However, biases inherent in surveys that select galaxies based on their star formation activity (e.g., Steidel et al. 2004) and stellar mass (e.g., Cimatti et al. 2002b; Glazebrook et al. 2004) can complicate such comparisons. Only with an accurate knowledge of the overlap between these samples can we begin to address the associations between galaxies selected in different ways, their mutual contribution to the SFRD at $z \sim 2$, and the prevalence and properties of passively evolving and massive galaxies at high redshift. Quantifying this overlap between optical and near-IR surveys is a primary goal of this paper.

In practice, optical surveys are designed to *efficiently* select galaxies with a specific range of properties. The imaging required for optical selection is generally a small fraction of the time required for near-IR imaging, and can cover much larger areas within that time. In contrast, near-IR surveys sample galaxies over a wider baseline in wavelength than optical surveys, and can include galaxies relevant to studying both the star formation rate and stellar mass densities at high redshift. However, in order to achieve a depth similar (and area comparable) to that of optical surveys, near-IR selection requires extremely deep imaging and can be quite expensive in terms of telescope time due to the relatively small size of IR arrays compared to CCDs. Furthermore, the "color" of the terrestrial background for imaging is $(B-K_{\rm s})_{\rm AB} \simeq 7$ magnitudes, much redder than all but the most extreme $z \sim 2$ galaxies. Once selected, of course, such extreme galaxies then require heroic efforts to obtain spectra, whereas optical selection, particularly at redshifts where key features fall shortward of the bright OH emission "forest," virtually guarantees that one can obtain a spectroscopic redshift with a modest investment of 8 - 10m telescope time and a spectrograph with reasonably high throughput. As we show below, optical and near-IR surveys complement each other in a way that is necessary for obtaining a reasonably complete census of galaxies at high redshift.

The SFRs of $z \sim 2$ galaxies are typically estimated by employing locally calibrated relations between emission at which the galaxies can be easily detected (e.g., UV, Hα) and their FIR emission. The X-ray luminosity of local non-active galaxies results primarily from high mass X-ray binaries, supernovae, and diffuse hot gas (e.g., Grimm et al. 2002; Strickland et al. 2004); all of these sources of X-ray emission are related to the star formation activity on timescales of $\lesssim 100$ Myr. Observations of galaxies in the local Universe show a tight correlation between X-ray and FIR luminosity, prompting the use of X-ray emission as an SFR indicator (Ranalli et al. 2003). This correlation between X-ray emission and SFR applies to galaxies with a very large range in SFRs, from $\sim 0.1 - 1000$ $M_\odot$ yr^{-1}. Stacking analyses at X-ray and radio wavelengths, and comparison with UV emission, indicate that the local SFR relations appear to give comparable estimates of the instantaneous SFRs of galaxies after assuming continuous star formation models and correcting for dust (e.g., Reddy & Steidel 2004; Nandra et al. 2002; Seibert et al. 2002).

Two surveys designed to select massive galaxies at redshifts $1.4 \lesssim z \lesssim 2.5$ and passively-evolving (PE) galaxies at redshifts $z \gtrsim 2$, respectively, are the K20 and FIRES surveys. The K20 and FIRES selection criteria were developed to take advantage of the sensitivity of rest-frame optical light and color to stellar mass and the strength of the Balmer break, respectively, for $z \sim 2$ galaxies (e.g., Cimatti et al. 2002a; Franx et al. 2003). The Gemini Deep Deep Survey (GDDS) extends this near-IR technique to target massive galaxies at slightly lower redshifts ($0.8 \lesssim z \lesssim 2.0$; Abraham et al. 2004).

X-ray stacking analyses of the brightest galaxies in the K20 and FIRES surveys indicate an average SFR a factor of 4 to 5 times larger than for optically-selected $z \sim 2$ galaxies (Daddi et al. 2004a; Rubin et al. 2004), inviting the conclusion that optical selection misses a large fraction of the star formation density at high redshift. While it is certainly true that optical surveys miss some fraction of the SFRD, the past quoted difference in the average SFRs of galaxies selected optically and in the near-IR disappears once the galaxies are subjected to a common near-IR magnitude limit, as we show below.

We have recently concluded a campaign to obtain deep near-IR imaging for fields in the $z \sim 2$ optical survey (Steidel et al. 2004), allowing for a direct comparison of optical and near-IR selected galaxies. One result of this comparison is that $K_{\rm s} < 20$ (Vega) optically-selected galaxies show similar space densities, stellar masses, and metallicities as $K_{\rm s}$-bright galaxies in near-IR samples (Shapley et al. 2004). More recently, Adelberger et al. (2005a) show that the correlation lengths for $K_{\rm s}$-bright galaxies among optical and near-IR samples are similar, suggesting an overlap between the two sets of galaxies, both of which plausibly host the progenitors of massive elliptical galaxies in the local Universe. These results suggest that near-IR bright galaxies have similar properties regardless of the method used to select them.

In this paper, we extend these results by examining the color distributions and X-ray properties of near-IR and optically selected galaxies at $z \sim 2$ in the GOODS-North field (Giavalisco et al. 2004b). The field is well-suited for this analysis given the wealth of complementary data available, including *Chandra*/X-ray, ground-based optical and near-IR, and *Spitzer*/IRAC imaging. Multi-wavelength data in a single field are particularly useful in that we can use a common method for extracting photometry that is not subject to the biases that may exist when comparing galaxies in different fields whose fluxes are derived in different ways. The addition of our rest-frame UV spectroscopic data in the GOODS-N field provides for a more detailed analysis than otherwise possible of the properties of galaxies as a function of selection technique. Furthermore, the GOODS-N field coincides with the *Chandra* Deep Field North (CDF-N) region which have the deepest (2 Ms) X-ray data available (Alexander et al. 2003). The X-ray data allow for an independent estimate of bolometric SFRs and the available depth allows more leeway in stacking smaller numbers of sources to obtain a statistical detection, as well as identifying AGN to a lower luminosity threshold than possible in other fields that have shallower X-ray data.

The outline of the paper is as follows. In § 2, we describe the optical, near-IR, X-ray, and IRAC data and present the optical and near-IR selection criteria and X-ray stacking method. Color distributions, direct X-ray detections, and stacked results are examined in § 3. In § 4, we discuss the SFR distributions of optical and near-IR selected $z \sim 2$ galaxies and their relative contributions to the SFRD, and the presence of a passively evolving population of galaxies. A flat ΛCDM cosmology is assumed with $H_0 = 70$ km s^{-1} Mpc^{-1} and $\Omega_\Lambda = 0.7$.

3.2 Data and Sample Selection

3.2.1 Imaging

Optical $U_{\rm n}G\mathcal{R}$ images in the GOODS-North field were obtained in April 2002 and 2003 under photometric conditions using the KPNO and Keck I telescopes. The KPNO/MOSAIC U-band image was obtained from the GOODS team (PI: Giavalisco) and was transformed to reflect $U_{\rm n}$ magnitudes (e.g., Steidel et al. 2004). The Keck I G and $\mathcal{R}$ band images were taken by us with the Low Resolution Imaging Spectrograph

(LRIS; Oke et al. 1995, Steidel et al. 2004), and were oriented to provide the maximum overlap with the GOODS ACS and *Spitzer* survey region. The images cover $11' \times 15'$ with FWHM $\sim 0\farcs7$ to a depth of $\mathcal{R} \sim 27.5$ ($3\ \sigma$). Image reduction and photometry were done following the procedures described in Steidel et al. (2003). We obtained deep B-band images of the GOODS-N field from a public distribution of *Subaru* data (Capak et al. 2004). The deep z-band data are acquired from the public distribution of the *HST* Advanced Camera for Surveys (ACS) data (Giavalisco et al. 2004b). The B and z band data have 5 σ depths of 26.9 and 27.4 mag measured in 3 $''$ and $0\farcs2$ diameter apertures, respectively. The $K_{\rm s}$ and J imaging was accomplished with the Wide Field Infrared Camera (WIRC) on the Palomar Hale 5 m telescope (Wilson et al. 2003), providing $8\farcm7 \times 8\farcm7$ coverage in the central portion of the GOODS-N field. The near-IR images cover $\sim 43\%$ of the optical image. The images had FWHM $\sim 1\farcs0$ under photometric conditions and 3 σ sensitivity limits of ~ 22.6 and ~ 24.1 mag in the $K_{\rm s}$ and J bands, respectively. The near-IR data are described in detail by Erb et al. (2006c). The total area studied in the subsequent analysis is ~ 72.3 arcmin^2.

The procedures for source detection and photometry are described in Steidel et al. (2003). Briefly, $U_{\rm n}G\mathcal{R}$ magnitudes were calculated assuming isophotal apertures that were adjusted to the $\mathcal{R}$-band flux profiles. Source detection was done at $K_{\rm s}$-band. BzK and J magnitudes are computed assuming the isophotal apertures adjusted to the $K_{\rm s}$-band flux profiles, unless the $\mathcal{R}$-band isophotes gave a more significant $K_{\rm s}$ detection. In the analysis to follow, "$K_{\rm s}$" and J magnitudes are in Vega units. We use the conversion $K_{\rm AB} = K_{\rm s} + 1.82$. All other magnitudes are in AB units.

Fully reduced *Spitzer*/IRAC mosaics of the GOODS-North field were made public in the first data release of the GOODS Legacy project (PI: Dickinson). The IRAC data overlap completely with our $K_{\rm s}$-band image, but currently only two channels (either 3.6 μm and 5.8 μm, or 4.5 μm and 8.0 μm) are available over most of the image. A small area of overlap has coverage in all four channels. The images are deep enough that source confusion is an issue. We have mitigated the effects of confusion noise by employing the higher spatial resolution $K_{\rm s}$-band data to constrain source positions and de-blend confused IRAC sources. We performed PSF photometry using the procedure described in Shapley et al. (2005).

3.2.2 Selection Criteria

3.2.2.1 Optical Selection of Star-Forming Galaxies

We have optically-selected $z \sim 2$ galaxies in the GOODS-N field based on their observed $U_nG\mathcal{R}$ colors (Adelberger et al. 2004; Steidel et al. 2004) to a limiting magnitude of $\mathcal{R} = 25.5$. The selection criteria aim to select actively star-forming galaxies at $z \sim 2$ with the same range in UV properties and extinction as LBGs at $z \sim 3$ (Steidel et al. 2003). "BX" galaxies are selected to be at redshifts $2.0 \lesssim z \lesssim 2.6$ using the following criteria:

$$\begin{aligned} G - \mathcal{R} &\geq -0.2 \\ U_n - G &\geq G - \mathcal{R} + 0.2 \\ G - \mathcal{R} &\leq 0.2(U_n - G) + 0.4 \\ U_n - G &\leq G - \mathcal{R} + 1.0, \end{aligned} \tag{3.1}$$

and "BM" objects are selected to be at redshifts $1.5 \lesssim z \lesssim 2.0$ using the following criteria:

$$\begin{aligned} G - \mathcal{R} &\geq -0.2 \\ U_n - G &\geq G - \mathcal{R} - 0.1 \\ G - \mathcal{R} &\leq 0.2(U_n - G) + 0.4 \\ U_n - G &\leq G - \mathcal{R} + 0.2 \end{aligned} \tag{3.2}$$

(Adelberger et al. 2004; Steidel et al. 2004). For subsequent analysis, we will refer to BX and BM objects as those that are optically-, or "BX/BM"-, selected.

Optical color selection of $z \sim 2$ galaxies in the $11'$ by $15'$ area of the GOODS-North field yielded 1360 BX and BM candidates, of which 620 lie in the region where we have complementary $J-$ and K-band data (§ 3.2.1), and 199 have $K_s < 21.0$. Followup spectroscopy with the blue channel of the Low Resolution Imaging Spectrograph (LRIS-B) yielded 147 redshifts for objects with K_s-band data (248 redshifts over the entire optical field). Of these 147 objects with redshifts and K_s-band data, 129 have $z > 1$, and 60 have $z > 1$ *and* $K_s < 21$. The mean redshift of the 60 BX/BM objects is $\langle z \rangle = 1.99 \pm 0.36$. The spectroscopic interloper fractions in the BX/BM sample are summarized in Table 3.1. The BX and BM selection functions (shown as shaded distributions in Figure 3.1) have distributions with mean redshifts $\langle z \rangle = 2.2 \pm 0.3$ and $\langle z \rangle = 1.7 \pm 0.3$, respectively (Steidel et al. 2004), and the combination of these two samples comprise our BX/BM-selected $z \sim 2$ sample. In the analysis to follow, we designate an interloper as any object with $z < 1$.

3.2.2.2 Near-IR Selection of Star-Forming Galaxies

The near-IR properties of galaxies can be used both to target star forming galaxies and to identify those with extremely red colors that may indicate passive evolution. To address the former issue, we have employed the "BzK" selection criteria of Daddi et al. (2004a) to cull objects in the GOODS-N field and directly compare with those selected on the observed optical properties of $z \gtrsim 2$ galaxies. Daddi et al. (2004a) define the quantity "BzK":

$$BzK \equiv (z - K) - (B - z); \tag{3.3}$$

star-forming galaxies with $z > 1.4$ are targeted by the following criterion:

$$BzK \geq -0.2, \tag{3.4}$$

in AB magnitudes. Of the 1185 sources with $> 3\ \sigma$ B, z, and K detections and $K_s < 21$, 221 satisfy Equation 3.4. The surface density of BzK galaxies with $K_s < 21$ is ~ 3 arcmin^{-2}, similar to the surface density of BX/BM galaxies to a similar K_s-band depth. These star-forming BzK galaxies will be referred to as "BzK/SF" galaxies, and their spectroscopic redshift distribution *from our spectroscopic sample* is shown in Figure 3.1. Our deep near-IR imaging allows us to determine the redshift distribution for BzK/SF galaxies with $K_s > 20$ (and which also satisfy the BX/BM criteria), and the results are shown in Figure 3.2. The mean redshifts of the $K_s \leq 20$ and $K_s > 20$ distributions are $\langle z \rangle = 2.13 \pm 0.22$ and $\langle z \rangle = 2.03 \pm 0.41$, respectively, and agree within the uncertainty. We note, however, that the BzK/SF criteria select $K_s > 20$ objects over a broader range in redshift ($1.0 \leq z \leq 3.2$) than $K_s \leq 20$ objects. This reflects the larger range in BzK colors of $K_s > 20$ BzK/SF galaxies compared with those having $K_s \leq 20$. Additionally, the photometric scatter in colors is expected to increase for fainter objects, so a broadening of the redshift distribution for BzK/SF objects with fainter K_s magnitudes is not surprising.

We emphasize that we only know the redshifts for BzK/SF galaxies that also happen to fall in the BX/BM sample. In general, the true redshift distribution, $N_o^{BzK/SF}(z)$, of the BzK/SF sample will be broader than the distributions shown in Figure 3.1 and Figure 3.2, call them $N_c^{BzK/SF}(z)$), which are effectively convolved with the BX/BM selection function. For example, the rapid dropoff in $N_c^{BzK/SF}(z)$ for $z > 2.6$ (Figure 3.2) may simply reflect the dropoff in the BX selection function for $z > 2.6$. However, the $N_c^{BzK/SF}(z)$ we derive here is similar to that of the *photometric* redshift distribution of K20 galaxies from Daddi et al. (2004a), which is subject to its own systematic errors, suggesting that a reasonable approximation is to take $N_o^{BzK/SF}(z) \simeq N_c^{BzK/SF}(z)$.

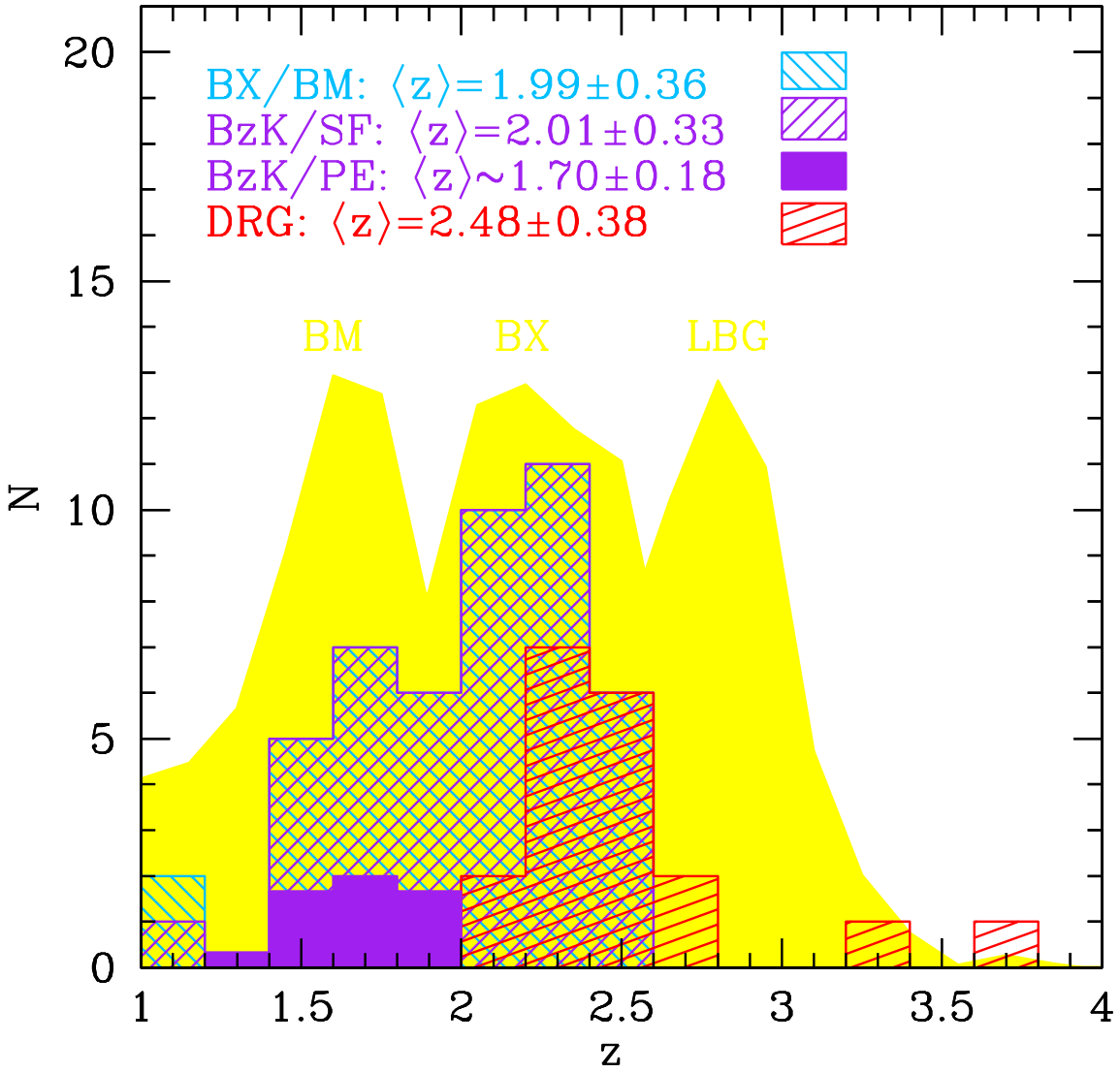

Figure 3.1 *Spectroscopic* redshift distributions to $K_s = 21$ for the various samples considered here. The BX/BM and BzK/SF distributions (hashed histograms) include sources from our sample in the GOODS-North field and overlap almost completely. The DRGs have a higher mean redshift of $\langle z \rangle = 2.48 \pm 0.38$ from our sample of $J - K_s > 2.3$ sources with $z > 1$ in all four fields of the optical survey (Steidel et al. 2004) where we have complementary $J-$ and K-band imaging. The redshift distribution of DRGs within our sample (all of which are selected with the BX/BM or $z \sim 3$ LBG criteria) is similar to that found by van Dokkum et al. (2004), van Dokkum et al. (2003), and Förster Schreiber et al. (2004b). The solid histogram shows the redshift distribution for BzK/PE galaxies from Daddi et al. (2004a) and Daddi et al. (2005b), scaled down by a factor of 3 for clarity. The background shaded regions show the arbitrarily normalized redshift distributions for optically-selected BX and BM galaxies, and LBGs.

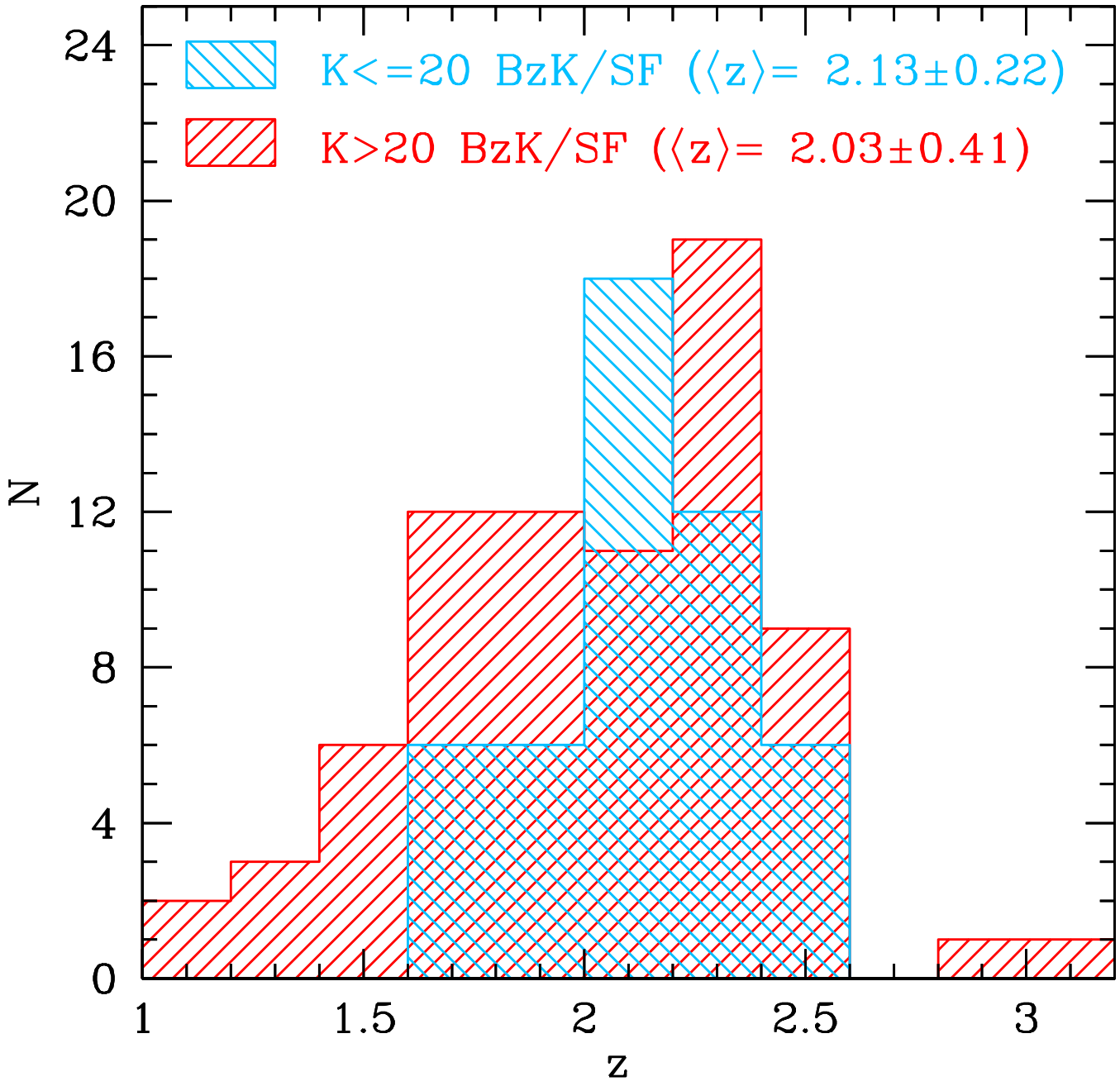

Figure 3.2 Arbitrarily normalized spectroscopic redshift distribution of BzK/SF galaxies in our spectroscopic sample to $K_s \sim 22.5$, with separate emphasis on $K_s \leq 20$ and $K_s > 20$ BzK/SF objects. The BzK/SF criteria select $K_s > 20$ objects over a broader range in redshift than $K_s \leq 20$ objects.

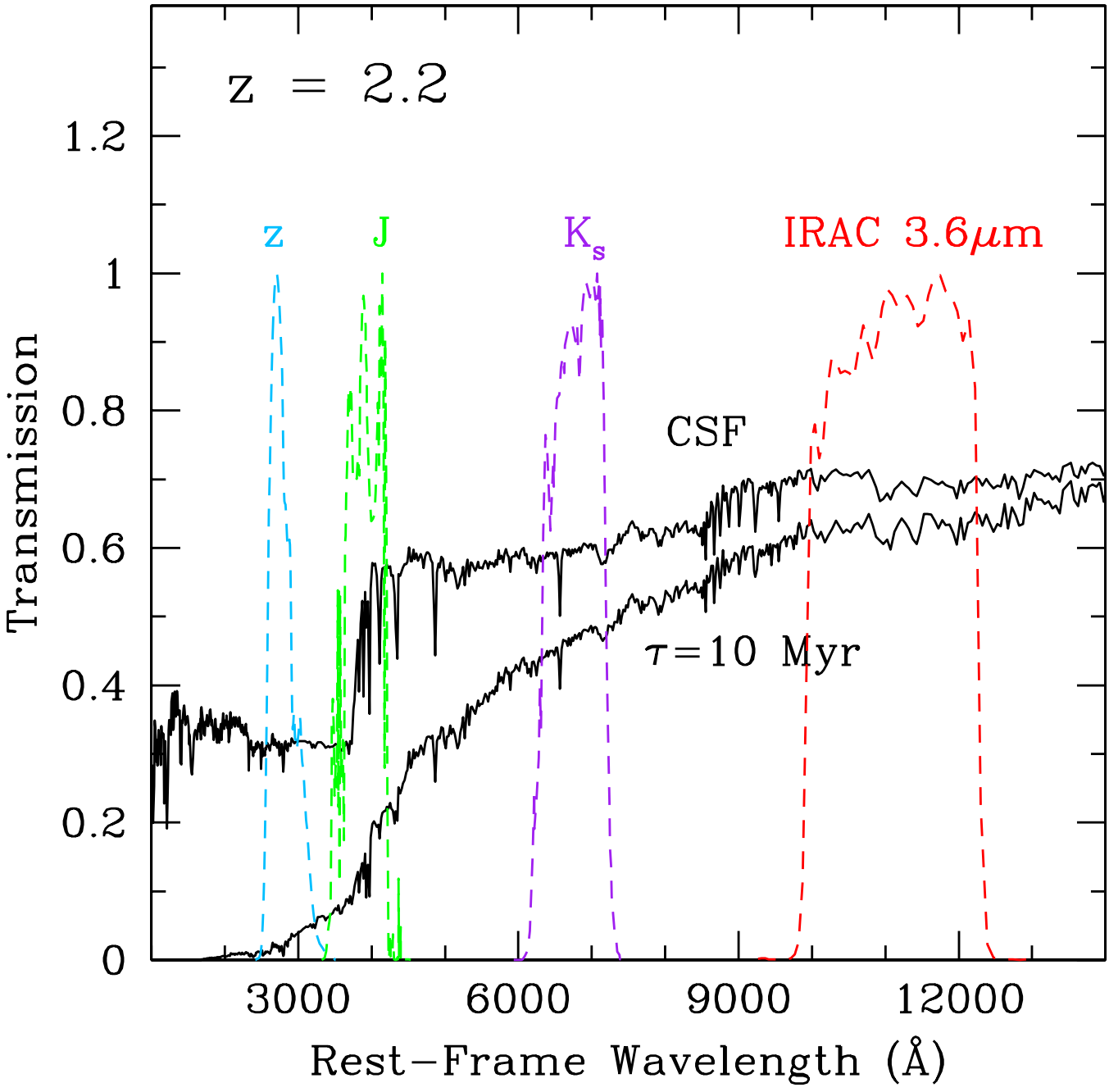

Figure 3.3 Relative transmission of the z, J, K_s, and IRAC 3.6 μm filters at rest-frame wavelengths for $z = 2.2$. Also shown are typical (unreddened) galaxy SEDs assuming constant star formation (CSF) and instantaneous star formation ($\tau = 10$ Myr) aged to 1 Gyr. For redshifts $z \sim 1.88 - 2.38$, the J-band brackets the prominent Balmer and 4000 Å breaks.

3.2.2.3 Near-IR Selection of Passively Evolving Galaxies

In addition to the criteria above, several methods have been developed to select passively evolving high redshift galaxies by exploiting the presence of absorption or continuum breaks in the SEDs of galaxies with

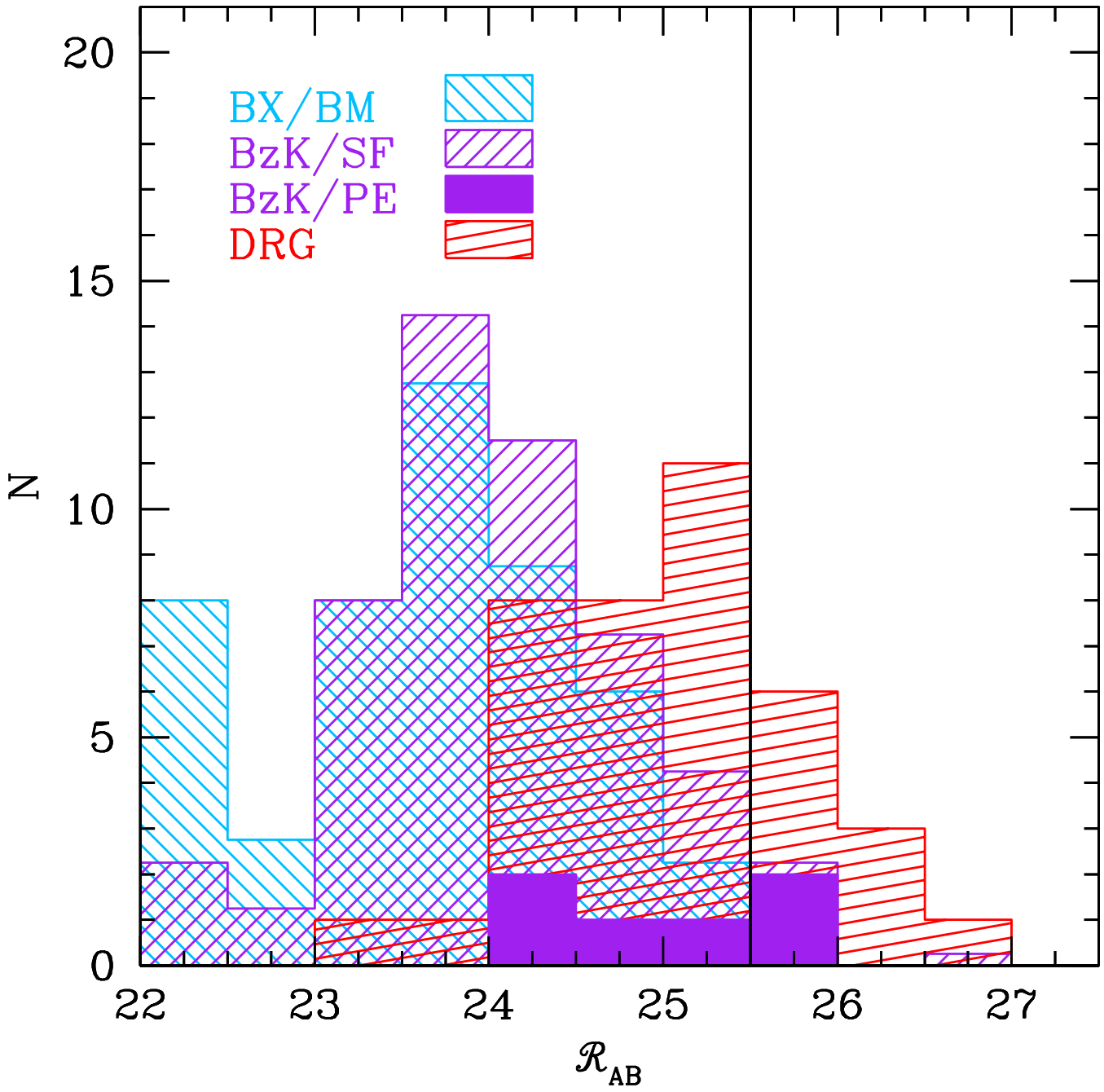

Figure 3.4 Optical magnitude distributions for photometrically selected $K_s < 21$ galaxies in the BX/BM, BzK, and DRG samples. The solid vertical line denotes the magnitude limit for galaxies in the optically-selected (BX/BM) sample. Approximately 47% of DRGs (34/73) have $\mathcal{R} > 27.0$ and are not shown in the figure. The distribution of BzK/PE galaxies has been arbitrarily normalized for clarity.